



# A snapshot of turbulence in the Northeastern Magellan Strait

Iossif Lozovatsky<sup>1</sup> · Cristian Escauriaza<sup>3</sup> · Leandro Suarez<sup>3,4</sup> · Harindra J. S. Fernando<sup>1,2</sup> · Megan Williams<sup>5</sup> · Ronald Scott Coppersmith<sup>1</sup> · Nicolas Mayorga<sup>3</sup>

Received: 27 October 2023 / Accepted: 28 March 2024 / Published online: 9 May 2024  
© The Author(s) 2024

## Abstract

First-ever measurements of the turbulent kinetic energy (TKE) dissipation rate in the northeastern Strait of Magellan (Segunda Angostura region) taken in March 2019 are reported here. At the time of microstructure measurements, the magnitude of the reversing tidal current ranged between 0.8 and 1.2 ms<sup>-1</sup>. The probability distribution of the TKE dissipation rate in the water interior above the bottom boundary layer was lognormal with a high median value  $\epsilon_{med}^{MS} = 1.2 \times 10^{-6}$  Wkg<sup>-1</sup>. Strong vertical shear,  $(1 - 2) \times 10^{-2}$  s<sup>-1</sup>, in the weakly stratified water interior ensued a sub-critical gradient Richardson number  $Ri < 10^{-1} - 10^{-2}$ . In the bottom boundary layer (BBL), the vertical shear and the TKE dissipation rate both decreased exponentially with the distance from the seafloor  $\xi$ , leading to a turbulent regime with an eddy viscosity  $K_M \sim 10^{-3}$  m<sup>2</sup>/s, which varied with time and location, while being independent of the vertical coordinate in the upper part of BBL (for  $\xi > \sim 2$  meters above the bottom).

**Keywords** Strait of Magellan · Segunda Angostura · Tidal Currents · Turbulence · BBL

## 1 Introduction

The Strait of Magellan (henceforth the Magellan Strait (MS) or just the Strait) is an environmentally unique region (Morris 1989), in particular, being a feeding ground to humpback whales (Acevedo et al. 2011). Expeditions through

Magellan passages are predicated by its complexity (with many fjords and dead ends) and foggy climate. The region currently experiences changes of its ecological balance due to anthropogenic stressors such as excessive fishing, offshore oil production and newly leased areas for aquaculture. Understanding of small-scale dynamical processes in the Magellan Strait waters is paramount for multidisciplinary studies of physical, biogeochemical and ecological processes in the coastal regions of Patagonia (Antezana and Hamamé, 1999). For this reason, we launched the first ever in-situ measurements of turbulence in the north-eastern part of the Strait on the water side to obtain estimates of the kinetic energy dissipation rate and eddy viscosity, which influence vertical transport of heat, momentum, nutrients, sediments and other substances, across the water column down to the seafloor.

The Strait of Magellan is a ~ 310 nautical miles (NM) long, narrow ~ 1.1 (NM) waterway that meanders between the Atlantic and Pacific oceans, separating Patagonia from Tierra del Fuego (Fig. 1). According to Simeoni et al. (1997), the mean annual air temperature of the eastern MS is 6–7° C, varying from 8° to 11 °C in the summer (December–February) and from 2° to 3° C in the winter (June–August). Easterly-directed winds of characteristic speed 7 ms<sup>-1</sup> are typical in the region (Garreaud et al. 2013).

---

Responsible Editor: Zhiyu Liu

---

Corresponding author: Iossif Lozovatsky<sup>+</sup> (Professor Lozovatsky unexpectedly passed away on 23 December, soon after the revisions of this paper were finalized).

---

✉ Harindra J. S. Fernando  
fernando.10@nd.edu

<sup>1</sup> Department of Civil & Environmental Engineering & Earth Sciences, University of Notre Dame, Notre Dame, USA

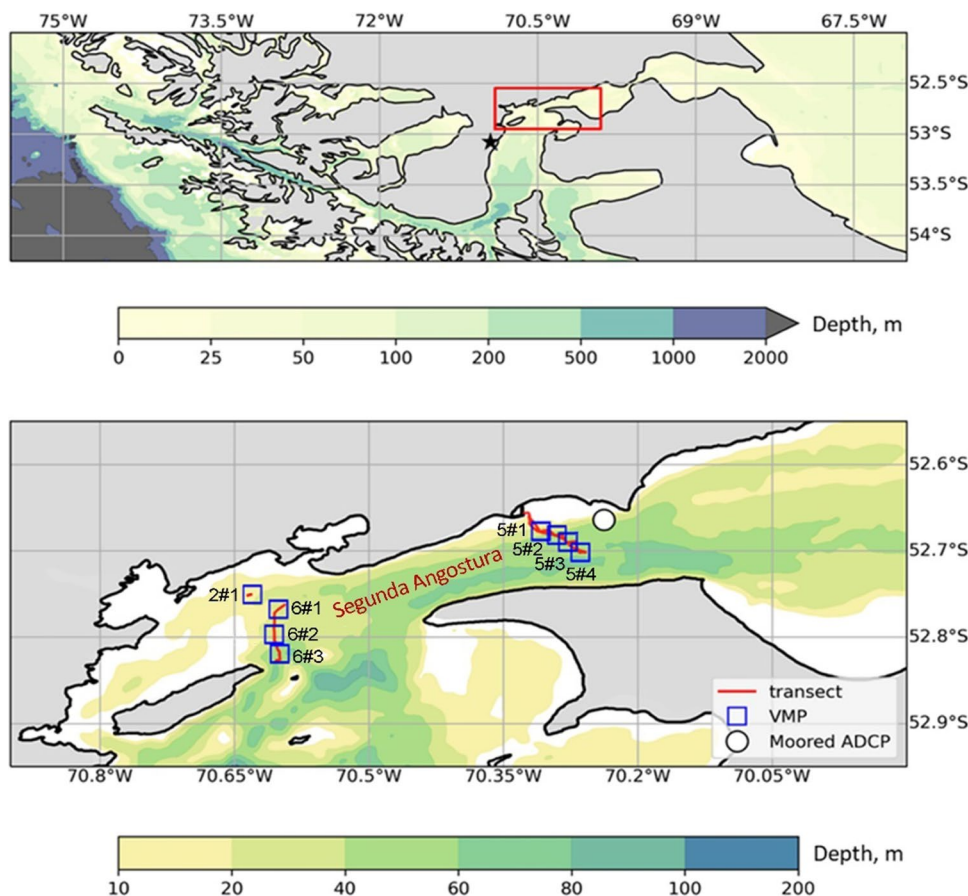
<sup>2</sup> Department of Aerospace and Mechanical Engineering, University of Notre Dame, Notre Dame, USA

<sup>3</sup> Departamento de Ingeniería Hidráulica y Ambiental, Pontificia, Universidad Católica de Chile, Región Metropolitana, Chile

<sup>4</sup> Marine Energy Research & Innovation Center (MERIC), Santiago, Chile

<sup>5</sup> Departamento de Obras Civiles, Universidad Técnica Federico Santa María, Valparaíso, Chile

**Fig. 1** Upper panel: the measurement site (bounded by a red box) in the main passage of the MS to the NNE from Punta Arenas (black star). Lower panel: an enlarged section of the MS showing locations of the VMP stations (squares marked by the station numbers); the ADCP mooring is a white circle). Two separate color palettes (scales) specify the mean water depth of the upper and lower panels, respectively. Segunda Angostura is a narrower channel in the Atlantic sector of the Magellan Strait



Stormy winds (up to  $25 \text{ ms}^{-1}$ ) are often observed during winter and spring seasons.

Strong barotropic tidal flow and winds are the major drivers of mesoscale circulation in the Strait. On the Atlantic side, the Strait is characterized by high-amplitude semidiurnal tides with a mean tidal range 7.1 m, which gradually decreases to about 1.5–2 m toward Punta Arenas (see Fig. 4 of Medeiros and Kjerfve 1988). Tidal amplification occurs in a series of narrows at the Atlantic side to the northeast of Punta Arenas (Fig. 1), for example, in Segunda Angostura (SA), where our pilot field campaign was conducted (see also detailed map of SA in Fig. 1 of Lutz et al. 2016). The seabed in SA is mainly composed of hard substratum and outcropping rocks (Simeoni et al. 1997). High level of tidally induced turbulence is an expected phenomenon in SA as has been reported in several recent publications on turbulence in narrow tidal channels elsewhere (e.g., Stevens and Smith 2016; McMillan et al. 2016; Horwitz and Hay 2017; Guerra and Thomson 2017; Ross et al. 2019).

Very limited information exists on hydrological characteristics of the Magellan waters. Antezana (1999) reported basic hydrographic features (temperature and salinity) in the main passages of the Strait and suggested that adjacent oceanic waters were warmest in the Atlantic and saltiest in

the Pacific sectors, maintaining an along-strait horizontal T-S gradient. Precipitation and continental freshwater discharge to the Strait induce patterns of diluted near surface waters transported to the Atlantic Patagonian shelf (Brun et al. 2020). The large-scale hydrological features as well as seasonal variations of mesoscale circulation may influence turbulence in the Strait, but strong tides and local winds are the most likely generators of turbulence in the shallow Atlantic sector of the MS.

To shed light on characteristics of small-scale turbulence in MS, a brief field campaign was carried out in the northeastern part of the Strait using a vertical microstructure profiler VMP-500 and acoustic Doppler current profilers (Sect. 2). Patterns of tidal currents during the microstructure measurements are described in Sect. 3.1. Sections 3.2 and 3.3 present several examples of TKE dissipation rate profiles, comparing the level of turbulence in well-mixed water interior of MS (Sect. 3.3) with turbulence intensity (illustrated by log-normal distribution functions of the dissipation rate) of homogeneous non-stratified layers in other kindred oceanic regions. Specifics of turbulence and mean current shear profiles in the BBL of Segunda Angostura are discussed in Sect. 3.4 vis-à-vis our own measurements carried out in various tidally affected shallow seas. The main

results are summarized in Sect. 4, including a comparison of turbulence measurements in narrow tidal channels found elsewhere. All times are in UTC.

## 2 Measurements

Turbulence and stratification in the Strait were measured using a Vertical Microstructure Profiler, VMP-500, (<http://rocklandscientific.com/products/profilers/vmp-500/>). Airfoil probes were used to estimate small-scale shear, enabling the calculation of TKE dissipation rate ( $\varepsilon$ ),  $z$  being the (downward) vertical coordinate. An accelerometer, pressure sensor and a SeaBird temperature-conductivity package provided precise salinity, temperature and potential density profiles. The airfoil sensors were calibrated by Rockland Scientific Inc. prior to and after the field campaign. The measurements were taken from a medium-size fishing boat, Marypaz II. The ship was equipped with A-frame at the rear deck, which was used to recover the VMP after each cast conducted in a free-falling mode with a thin tethered cable of neutral buoyancy. We were able to keep the VMP sinking velocity approximately constant,  $W \sim 0.7 \text{ ms}^{-1}$  (see Appendix), with casts usually terminated  $\sim 1\text{--}2$  m above the bottom.

A shipboard acoustic Doppler current profiler (ADCP) measured vertical profiles of zonal  $u(z)$  or  $u(\xi)$  and meridional  $v(z)$  or  $v(\xi)$  velocity components. Here,  $z$  is the distance from the sea surface,  $\xi = z_B - z$  the vertical distance above the sea floor (in meters; mab) and  $z_B$  the depth of the sea floor at the location of the measurements. A Teledyne Workhorse sentinel ADCP operated at 600 kHz with high vertical resolution (1-m bin size), but the measurements were restricted to the depth range  $z = 1\text{--}49$  m. Processing of the VMP and ADCP data followed well-established methodology adopted during our previous field campaigns (e.g., Lozovatsky et al. 2019, 2021; see also Roget et al. 2006 and Goodman et al. 2006). Multiple GPS systems were on board, but an automatic weather station was not present; thus, the meteorological conditions at Punta Arenas during the cruise were used as representative as local weather.

The VMP-500 was successfully deployed at eight stations (2–3 casts per station) near the eastern and western ends of Segunda Angostura (SA) of the Magellan Strait (Fig. 1). The first test station was taken on March 2 near the coast (the bottom depth  $z_B \sim 21$  m) under calm weather conditions (wind speed  $2\text{--}3 \text{ ms}^{-1}$ ). This appears to be the only VMP station wherein a weak but distinguishable temperature, salinity and density stratifications of the water column were observed. On March 3, a bottom-mounted ADCP mooring was setup in the northern part of SA (see Fig. 1), but the VMP measurements on March 3 and 4 were suspended due to rough seas (wave height up to 2 m) and high winds that periodically exceeded  $10\text{--}12 \text{ m s}^{-1}$ . Toward the end of the

day of March 5 the stormy wind ceased, allowing the conduct of four VMP stations in the central part of SA (closer to its eastern entrance,  $\varphi = 52^\circ 39'58''\text{--}52^\circ 42'7'' \text{ S}$ ,  $\lambda = 70^\circ 19'0''\text{--}70^\circ 15'51'' \text{ W}$ ; with  $z_B$  varying from 30 to 57 m). The measurements continued on March 6 at three stations across the Strait about four miles to the west off the western SA entrance ( $\varphi = 52^\circ 53'54''\text{--}52^\circ 49'5'' \text{ S}$ ,  $\lambda = 70^\circ 49'59''\text{--}70^\circ 38'58'' \text{ W}$  with  $z_B$  varying from 26 to 57 m). Positions of all VMP stations are shown in Fig. 1.

## 3 Results

### 3.1 Tidal flow

Basic tidal characteristics in the SA area of MS are given in Fig. 2 for two main days of VMP measurements (March 5–6, 2019). The ADCP current components  $u(\zeta, t)$  and  $v(\zeta, t)$  at the mooring location are shown in Fig. 2a and the tidal elevation  $\eta_{td}(t)$  and tidal ellipses are in Fig. 2b. It appears that a semidiurnal tide ( $\omega_{td} = 1.41 \times 10^{-4} \text{ s}^{-1}$ ) with current amplitude  $\sim 2 \text{ ms}^{-1}$  and surface elevation  $\sim 1.5$  m was a dominant background force governing mean currents that generated small-scale turbulence in the SA region. The tidal ellipses (Fig. 2b) are highly stretched in NE–SW direction along the SA axis in the middle of the narrow channel.

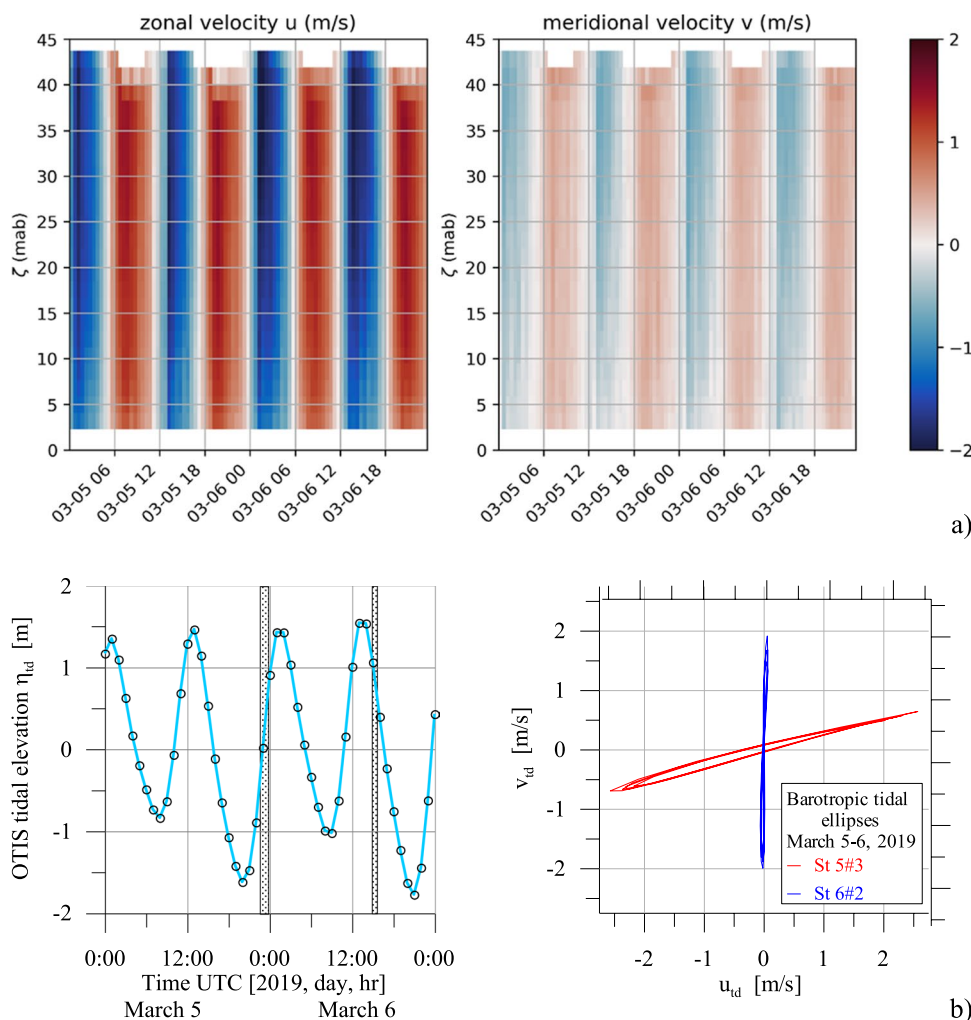
To the west of SA, the dominant tidal current was in the S–N direction with a large meridional component (amplitude  $v_{td} \approx \pm 2 \text{ ms}^{-1}$ ) and a very small zonal component ( $u_{td} \approx \pm 0.07 \text{ ms}^{-1}$ ). Note that the VMP measurements were taken during rising tide on March 5 and falling tide on March 6, but not at the periods of maximum tidal velocities due to the operational constrains.

### 3.2 MS turbulence: stable ambient stratification

Figure 3 shows the TKE dissipation rate profile  $\varepsilon(\xi)$  obtained on March 2 at the beginning of the field campaign under light winds ( $2\text{--}3 \text{ ms}^{-1}$ ).

The background density stratification was characterized by  $N^2 \sim 2 \times 10^{-5} \text{ s}^{-2}$  for the upper weakly stratified 5 m of the water column ( $\xi > 16$  mab), increasing to  $\sim 6 \times 10^{-5} \text{ s}^{-2}$  in a narrow,  $\xi = 13\text{--}16$  mab, pycnocline (thermocline). Then it generally decreased to  $N^2 \sim (0.9\text{--}2)10^{-5} \text{ s}^{-2}$  below the pycnocline ( $\xi < 11\text{--}12$  mab). The TKE dissipation rate profile shows relatively high  $\varepsilon \approx (1\text{--}2) \times 10^{-7} \text{ W kg}^{-1}$  in the near surface layer, decreasing to  $\varepsilon \sim 10^{-8} \text{ W kg}^{-1}$  in the pycnocline. Starting from  $\xi \sim 6$  mab, however,  $\varepsilon(\xi)$  clearly exhibited an exponential growth toward the seafloor (black line in Fig. 3), reaching  $\varepsilon \sim 8 \times 10^{-7} \text{ W kg}^{-1}$  at  $\xi \sim 3$  mab. Note that at this station the VMP did not descend closer to the [shallow] bottom, where  $\varepsilon$  could perhaps rise by another order of magnitude. The TKE dissipation in the interior of

**Fig. 2 a)**—ADCP current components at the mooring location (see Fig. 1) for March 5–6, 2019 (color scale in  $\text{m s}^{-1}$ ; **b)** left—tidal elevation in SA based on modeling data of OTIS (OSU Tidal Inversion Software, courtesy of S. Erofeeva; <https://www.tpxo.net/otis>). Periods of VMP measurements are marked by grey segments; **b)** right – OTIS barotropic tidal ellipses in SA for St.5#3 and St. 6#2



stratified water column,  $\epsilon \sim (1 - 3) \times 10^{-8} \text{ W kg}^{-1}$ , appears to be comparable with (but at the higher end of) the dissipation estimates obtained in our previous measurements on shallow stratified *tidal* shelves elsewhere (see  $\epsilon(\xi)$  profiles presented later in Fig. 7). Note that even in narrow tidal channels, for example, Sansum Narrows that separates Vancouver and Saltspring Islands in British Columbia, Canada with flooding tide of  $\sim 2 \text{ m s}^{-1}$ , turbulence is strongly affected by layers of stable stratification, decreasing  $\epsilon$  to  $< 10^{-8} \text{ W kg}^{-1}$  (Wolk and Lueck 2012).

### 3.3 MS turbulence: well-mixed water interior

After stormy winds with speeds 10–12  $\text{m s}^{-1}$  on March 4, the water column in SA was almost completely mixed; see temperature  $T(z)$ , salinity  $S(z)$ , potential specific density  $\sigma_\theta(z)$  and the dissipation rate  $\epsilon(z)$  profiles given in Fig. 4 for two deepest stations 5#4 and 6#3 of each transect, which are characterized by very low  $N^2$  with the mean  $\langle N^2 \rangle$  close to  $10^{-6} \text{ s}^{-2}$ .

Owing to a limited depth range of the ship-based ADCP measurements ( $z_{\text{max}} = 49 \text{ m}$ ), dynamical characteristics of well-mixed tidal flow in the MS, including BBL, are demonstrated in Fig. 5 at two shallower stations 5#1 and 6#2. These are vertical profiles of  $N^2(\xi)$ ,  $Sh^2(\xi)$  (the squared vertical shear), the gradient Richardson number  $Ri(\xi) = N^2(\xi)/Sh^2(\xi)$  and  $\epsilon(\xi)$ . Note that the vertical structure of all variables in Fig. 5 exhibits two distinct layers. The first is the bottom boundary layer, where the dissipation rate exponentially increases with depth ( $\xi < \xi_{BBL} \approx 7 - 8 \text{ mab}$ ) mirroring an exponential increase of vertical shear and corresponding decrease of  $Ri(\xi)$ . Although  $N^2(\xi)$  shows slight increase at 2 m above the seafloor, the values of  $N^2 < 7 \times 10^{-7} \text{ s}^{-2}$  are still extremely low.

Another major layer covers the water column above the BBL ( $\xi > \xi_{BBL}$ ), where the shear and the dissipation rate vary around the means  $\langle \epsilon \rangle = 6.8 \times 10^{-7} \text{ W kg}^{-1}$  and  $\langle Sh^2 \rangle = 1.1 \times 10^{-4} \text{ s}^{-2}$ , for an example in Fig. 5b.

The statistical behavior of such random variable as  $\epsilon$  can be specified in terms of the cumulative probability distribution function  $CDF(\epsilon)$ , shown in Fig. 6 by red pentagrams,

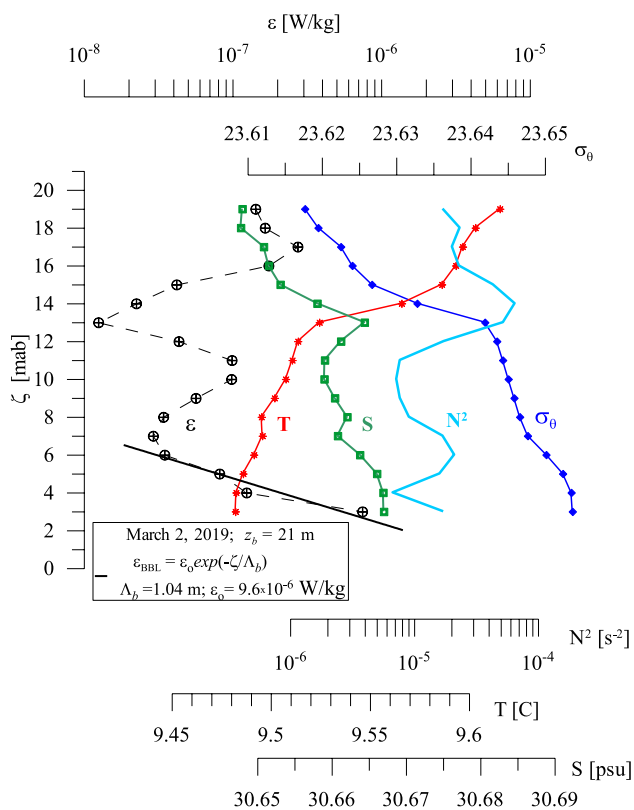
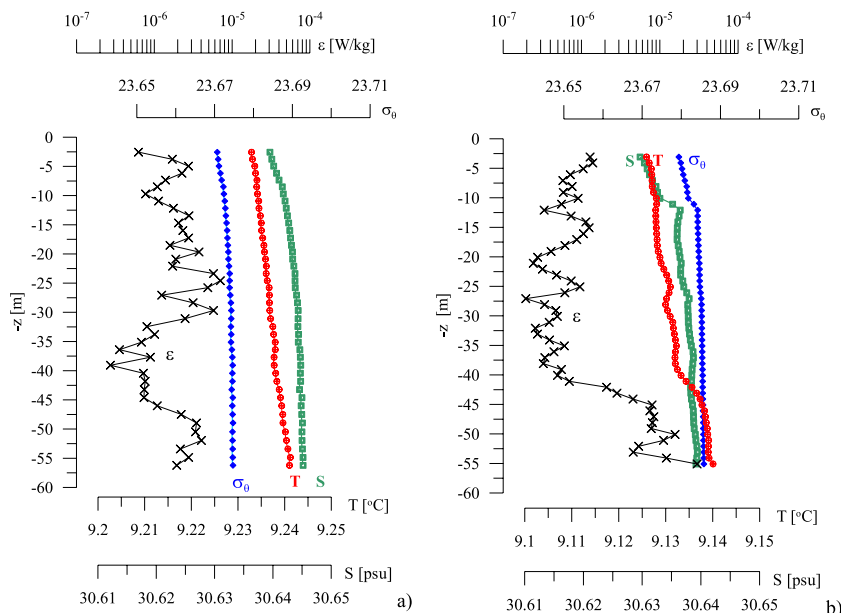


**Fig. 3** Profiles of the TKE dissipation rate  $\epsilon(\xi)$ , temperature  $T(\xi)$ , salinity  $S(\xi)$ , potential specific density  $\sigma_\theta(\xi)$ , and squared buoyancy frequency  $N^2(\xi)$  observed under light winds to the west from SA (station 2#1 in Fig. 1). Here  $\xi$  is the distance above the bottom in meters (mab). The mean flow speed was  $0.3 \text{ ms}^{-1}$

**Fig. 4** Temperature  $T(z)$ , salinity  $S(z)$ , potential specific density  $\sigma_\theta(z)$  and the dissipation rate  $\epsilon(z)$  profiles at two deepest MS stations 5#4 (a) and 6#3 (b). The scales of the variables are identical in both panels. The mean flow speed for stations 5#4 and 6#3 was, respectively,  $0.9 \text{ m s}^{-1}$  and  $1.1 \text{ m s}^{-1}$



calculated using all dissipation samples pertained to the depth range between  $z_o = 5$  m and  $z_{BBL} = 25\text{--}50$  m depending on the BBL height  $\xi_{BBL}$  in every specific VMP cast. To compare turbulence intensity in homogeneous waters of MS with non-stratified turbulence in oceanic regions elsewhere, Fig. 6 shows several examples of  $CDF(\epsilon)$  obtained for surface mixed layers (SML) in the northern (Jinadasa et al. 2016) and southwestern (Lozovsky et al. 2019) Bay of Bengal (BoB-13 and BoB-18, in 2013 and 2018, respectively) and in the Gulf Stream region in 2015 (GS-15). Those  $CDF(\epsilon)$  were calculated for  $z = 10$  to 30 m for relatively shallow SML underlain by a sharp pycnocline in both BoB regions under moderate local winds and  $z = 10$  to 50 m in a deep, well-developed SML for GS-15 (Lozovsky et al. 2017a).

As expected from numerous previous results obtained in non-stratified marine layers (e.g., Lozovsky et al. 2017b; McMillan and Hay 2017), all  $CDFs(\epsilon)$  in Fig. 6 are well approximated by lognormal probability distribution model of Gurvich and Yaglom (1967). Furthermore, Fig. 6 indicates that turbulence in SA is much stronger than that typically observed in oceanic SML under similar (low and moderate) winds. The median value of the TKE dissipation rate in the MS above the BBL  $\epsilon_{med}^{MS} = 1.2 \times 10^{-6} \text{ W kg}^{-1}$  is an order of magnitude higher than that in SML  $CDFs$  shown in Fig. 6, where  $\epsilon_{med}^{SML} \approx (2 - 7) \times 10^{-7} \text{ W kg}^{-1}$ . Such high level of turbulence appears to be governed by shear instability developed over the entire water column in the SA region, where  $med(Sh^2) = 1.2 \times 10^{-4} \text{ s}^{-2}$  and  $Ri$  values are highly subcritical, varying above the BBL mostly in the range  $Ri \sim 0.01 - 0.1$  with the mean  $\langle Ri \rangle = 0.033$  for 0.5#1, 5#2, 6#1, and 6#2.

**Fig. 5** Example of the vertical profiles of  $N^2(\zeta)$  and  $Sh^2(\zeta)$ ,  $Ri(\zeta)$ , and  $\epsilon(\zeta)$  obtained on March 5 (a) and March 6 (b) in the mixed waters of MS (signified by very small values of  $N^2(\zeta) \sim 10^{-6} \text{ s}^{-2}$  across the entire water column). Stations 5#1 (a) and 6#2 (b) are shown in Fig. 1

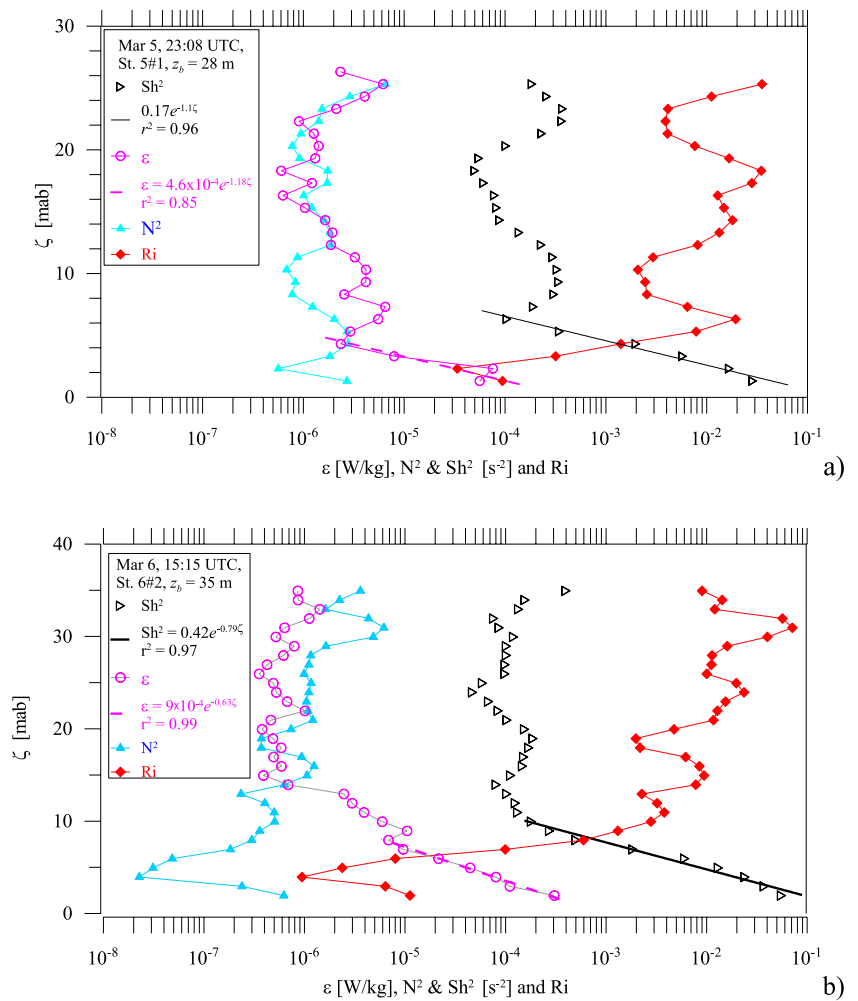
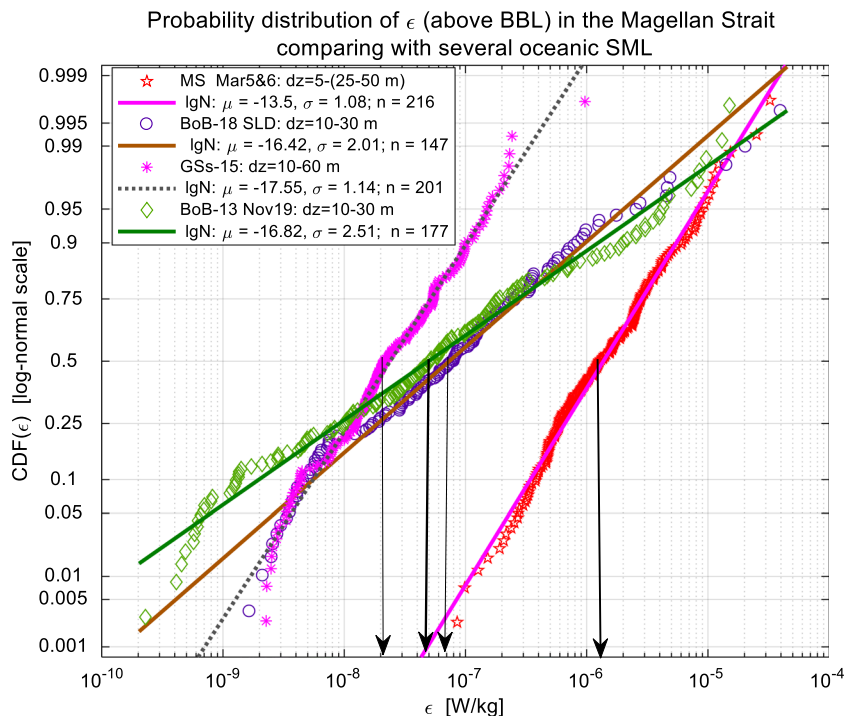


**Fig. 6** Cumulative distribution functions of the dissipation rate  $CDF(\epsilon)$  for mixed water interior of the Magellan Strait (March 5–6 data) and examples of  $CDF(\epsilon)$  for oceanic surface mixed layer (SML) under light and moderate winds. The measurements were taken in the northern and southern Bay of Bengal (BoB-13 and BoB-18, respectively) and in the Gulf Stream (GS-15). The depth ranges selected for  $CDF(\epsilon)$  calculation, the number of CDF samples  $n$  and parameters of lognormal approximations of the empirical distributions  $\mu$  and  $\sigma$  are in the legend. The arrows point to the corresponding median values



### 3.4 MS turbulence: BBL

The BBL in well-mixed waters of MS was not distinct in thermohaline profiles due to very small differences in temperature, salinity, and density near the bottom, but the BBL was easy to define in the profiles of the squared mean shear  $Sh^2(\xi)$  and the dissipation rate  $\epsilon(\xi)$ . The TKE dissipation profiles  $\epsilon(\xi)$  shown in Figs. 5a,b clearly indicate that starting from some distance above the bottom  $\xi_{BBL} = z_b - z_{BBL}$ , the dissipation rate sharply (exponentially) increases toward the seafloor. All  $\epsilon(\xi)$  profiles in the MS showed an exponential dependence  $\epsilon$  on  $\xi$

$$\epsilon(\xi) = \epsilon_b e^{-\xi/\Lambda} \tag{1}$$

where  $\epsilon_b$  is the dissipation rate near the bottom and  $\Lambda$  a characteristic external length scale for shear generated turbulence by mean (tidal) flow. Two additional  $\epsilon(\xi)$  profiles typical of March 5 and 6 are given in Fig. 7 along with several profiles of  $\epsilon(\xi)$  obtained elsewhere in shallow tidal seas, where an exponential decrease of  $\epsilon$  with  $\xi$  in BBL is demonstrated. These latter data were collected in the Changjiang River Diluted Waters (YS-CDW) in the southwestern Yellow Sea (Lozovatsky et al. 2012), in the IEODO region (YS-IEODO) in the southeastern Yellow Sea (Lozovatsky et al. 2015) as well as on the North Carolina (NC) shelf (Lozovatsky et al.

2017a). Note that an exponential decay of  $\epsilon(\xi)$  with  $\xi$  has been suggested by St. Laurent et al. (2002) for deep-ocean BBL as a possible model of  $\epsilon(\xi)$  for the case of turbulence generated by internal tidal energy propagated upward over rough abyssal bathymetry. According to St. Laurent et al. (2002) this choice was motivated by turbulence observations in the abyssal ocean (St. Laurent et al. 2001) and on continental slope (Moum et al. 2002) that suggested exponential decay of TKE dissipation rate away from the topography. Our  $\epsilon(\xi)$  measurements are taken in weakly stratified waters at much shallower depths, which also exhibit an exponential decrease of in the BBL. This observation is related to an exponential increase of vertical shear toward the bathymetry (see Fig. 5 and also Fig. 8). The observed decay could be interpreted in light of faster (exponential) decay of turbulence observed at the sloping side-walls of the underwater canyons, like Segunda Angostura (Fig. 5), considering resemblance between the present topography with flatter “valley” at the center of such canyons.

All dissipation rate profiles in shallow BBL shown in Fig. 7 can be well approximated by formulae (1) with coefficient of determination  $r^2 = 0.93$ – $0.99$ . The tallest turbulent BBL with exponentially varying  $\epsilon(\xi)$  was observed in the YS-IEODO region ( $\xi_{BBL} \sim 15$  mab,  $\Lambda = 3.1$  m) while a characteristic height of such BBL in other regions was  $\xi_{BBL} \sim 7$ – $9$  mab with  $\Lambda = 1.4$ – $1.9$  m. It is worth noting that for

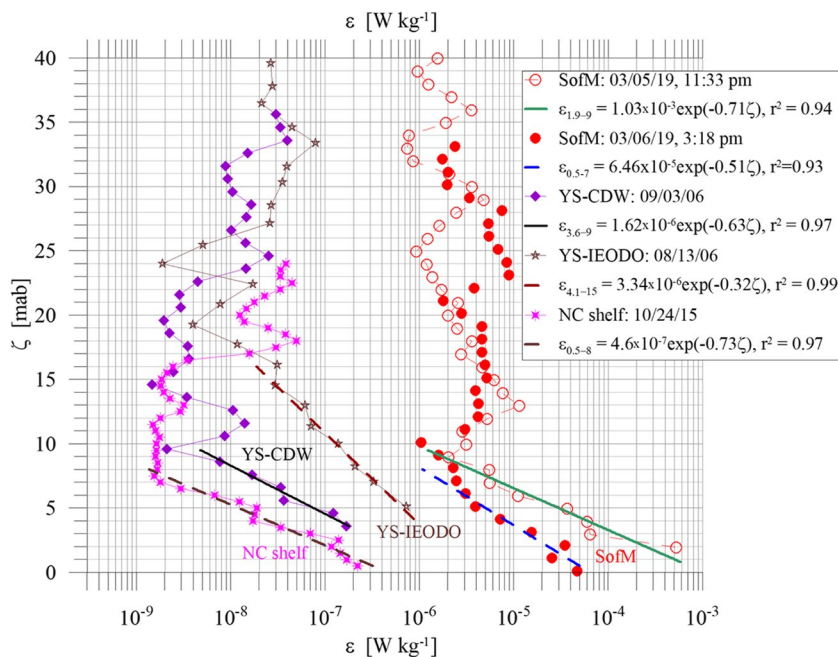


**Fig. 7** Examples of  $\epsilon(\xi)$  profiles showing an exponential increase of  $\epsilon$  in the MS BBL toward the seafloor at two stations in the Strait (5#3 and 6#3) and typical  $\epsilon(\xi)$  profiles measured not in MS, but in shallow tidal seas elsewhere that exhibit exponential dependences  $\epsilon(\xi) \sim \epsilon_b \exp(-\xi/\Lambda)$  in BBL. Here,  $\epsilon_b$  is a characteristic dissipation rate and  $\Lambda$  a characteristic length-scale of BBL turbulence. Those

data have been reported by Lozovatsky et al. (2017a) for North Carolina shelf (NC shelf) and by Lozovatsky et al (2012, 2015) for Changjiang River Diluted Waters (YS-CDW) in the southwestern sector of Yellow Sea, and for the IEODO region (YS-IEODO) in the southeastern YS, respectively. Parameters pertinent to the exponential approximations  $\epsilon(\xi)$  (straight lines) are in the legend

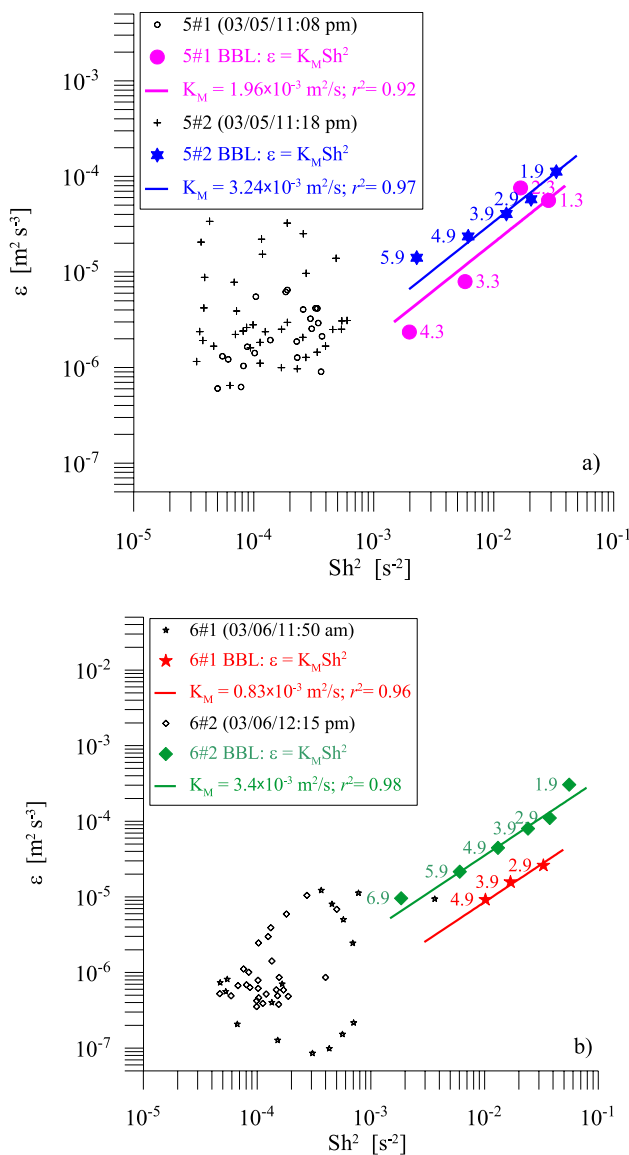


**Fig. 8** The TKE dissipation rate  $\epsilon$  vs. the squared vertical shear  $Sh^2$ : **a**)—stations 5#1 and 5#2, **b**)—stations 6#1 and 6#2. Colored enlarged symbols belong to BBLs (see examples in Figs. 5 and 7); the numbers adjacent to the symbols specify the height above the bottom in mab. Parameters pertinent to the approximations by Eq. 2 (eddy viscosity and  $r^2$ ) are in the legend

all  $\epsilon(\xi)$  profiles in Fig. 7, the external turbulent scale can be evaluated as  $\Lambda \sim 0.2\xi_{BBL}$ , which is typical for boundary-induced turbulence (e.g., Monin and Yaglom 1971). An exponential decrease of  $\epsilon(\xi)$  within the YS-IEODO BBL has been observed by Lozovatsky et al. (2015) who argued that weak remnant stable stratification therein could cause a faster decrease of  $\epsilon$  with  $\xi$  compared to an inverse-distance decay of  $\epsilon(\xi)$  that has been discussed in some publications (e.g., Sanford and Lien 1999; Lozovatsky et al. 2008; McMillan et al 2016) in relation to marine BBL.

While such an assumption for the MS BBL with very small  $N^2 \approx 10^{-7} - 10^{-6} \text{ s}^{-2}$  should be considered with circumspection, Sakamoto and Akitomo (2006) argued that even weakly stable stratification on the order of  $N^2 \approx 10^{-6} \text{ s}^{-2}$  may suppress BBL mixing specifically at high latitudes. Rotation of tidal flow may also have a stabilizing effect on BBL turbulence, similar to stable stratification and/or the Coriolis forces (e.g., Sakamoto and Akitomo 2008; Yoshikawa et al. 2010). Tidal ellipses in the SA region are so narrow (Fig. 2b), however, that the flow resembles a reversing rather than a rotating tide.

In general, it is plausible that the exponential decay of  $\epsilon(\xi)$  in the MS BBL and in several tidal shallow seas with bathymetric irregularities may have different dynamical origins vis-à-vis stationary [classical] log-layer boundary turbulence, with latter exhibiting  $\epsilon = u_*^3/\kappa\xi$ , with  $u_*$  is friction velocity and  $\kappa$  is von-Karman constant (e.g., Pedlosky 1987). Yet they show similar behaviors due to exponential increase of mean squared shear in the BBL, which was presented in Fig. 5a, b. To verify the dependence between shear and dissipation rate, we plotted  $\epsilon$  vs.  $Sh^2$  for MS stations with  $z_b < 49 \text{ m}$ , where both VMP and ADCP provided data close to the seafloor (1.3 – 2.9 mab). The data from “exponential BBLs” are shown in Fig. 8 by large symbols with adjacent numbers indicating the height from the seafloor. If turbulence is solely generated by mean shear, for stationary turbulence the production  $K_M Sh^2$  term is balanced by viscous dissipation  $\epsilon$  as

$$K_M Sh^2 = \epsilon \tag{2}$$

where  $K_M$  is the eddy viscosity that parametrizes the vertical momentum flux  $u'w' = -K_M Sh$ . In Fig. 8, the success of Eq. 2 as an approximate empirical regression between  $\epsilon$  and  $Sh^2$  in the BBLs is apparent with high coefficients of determination  $r^2 = 0.92 - 0.98$ . The result suggest that in the MS BBL (at  $\xi > \sim 2 \text{ mab}$ ), the eddy viscosity  $K_M$  is independent of  $\xi$  (constant with height), varying in a relatively narrow range  $K_M = (0.83 - 3.4) \times 10^{-3} \text{ m}^2 \text{ s}^{-1}$ , though it depends on the location in the Strait and the time of measurement (i.e., tidal phase); also see Ross et al. (2019) who reported substantial tidal variability of  $K_M$  in a coastal plain estuary in the French Atlantic Coast. Note that on March 5 and March 6, the VMP measurements were taken in approximately the same transitional phase between low and high tide indicated in Fig. 2.

The estimates of  $K_M$  allow assessing the possible thickness of the turbulent BBL  $h_{tbl}$  over a bottom roughness. Yoshikawa et al. (2010) suggested that rotating tidal currents over a large continental shelf affect the thickness of the Ekman BBL.

Considering, however, that background rotation associated with strong reversing tidal currents is negligible in such



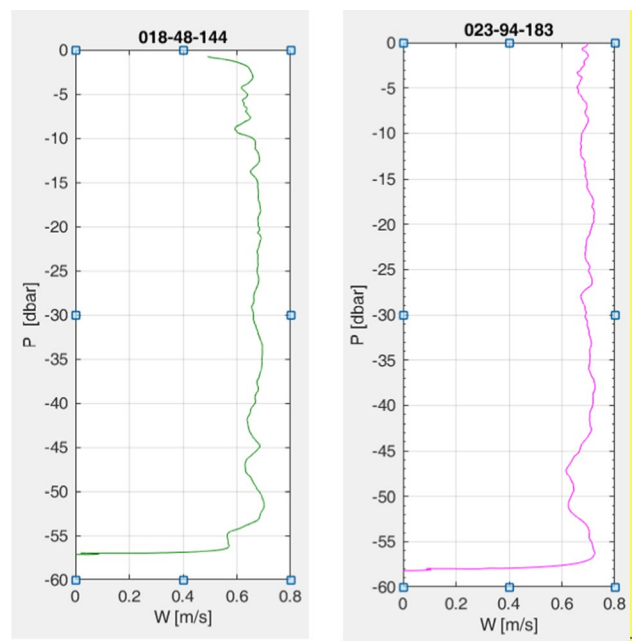
narrow channels as SA, it is not possible to use the classical Ekman BBL height formulae in this case (Pedlosky 1987), wherein the Stokes oscillatory boundary layer (e.g., Krstic and Fernando 2001) formula is more appropriate. Accordingly, the thickness of the reversing tidal turbulent BBL  $h_{tbl}$  over rough bathymetry composed of hard substratum (Simeoni et al. 1997) can be written as

$$h_{tbl} = \left( \frac{2K_M}{\omega_{td}} \right)^{1/2} \tag{3}$$

where  $\omega_{td} = 1.41 \times 10^{-4} \text{ s}^{-1}$  the semidiurnal tidal frequency. Using the estimates for the present case  $K_M = (0.83 - 3.4) \times 10^{-3} \text{ m}^2\text{s}^{-1}$ ,  $h_{tbl}$  is found to be in the range 3.5 – 6.9 m. This is in general agreement with data shown in Fig. 8, where the height of the “exponential BBL” varies between 4.3 and 6.9 mab. Thus, reversing tidal currents in a channel of the ilk of SA may create a specific regime of strong ( $\epsilon_b \sim 10^{-3} \text{ Wkg}^{-1}$ ) bottom-generated turbulence, which can be characterized by a constant eddy viscosity and a TKE dissipation rate that exponentially decays toward the water interior. The upper boundary of the exponential decay region of turbulence in the northern MS is 4–7 mab for a characteristic tidal velocity  $\sim 1 \text{ m s}^{-1}$  and eddy viscosity  $\sim 10^{-3} \text{ m}^2 \text{ s}^{-1}$ .

### 4 Conclusions

First ever measurements of turbulence in the northeastern Strait of Magellan were conducted during March 2 – 6, 2019. A vertical microstructure profiler (VMP) and a shipboard acoustic Doppler current profiler (ADCP) were used to obtain estimates of the TKE dissipation rate and vertical shear at several stations (the bottom depth ranged between 25 and 55 m), respectively, in the Segunda Angostura region to the north of Punta Arenas. During the campaign, tidal elevation varied in the range  $\pm \sim 1.5 \text{ m}$ . At the time of microstructure measurements, the speed of reversing tidal currents was 0.8–1.2  $\text{m s}^{-1}$ . After a mild storm, entire water column became well mixed with the median TKE dissipation rate above the bottom boundary layer  $\epsilon_{med}^{MS} = 1.2 \times 10^{-6} \text{ W kg}^{-1}$ , which was about an order of magnitude higher compared to the surface mixed-layer turbulence measured under moderate winds in typical ocean. This was associated with strong,  $(1 - 2) \times 10^{-2} \text{ s}^{-1}$ , vertical shear in the water interior that yielded gradient Richardson numbers  $Ri < 10^{-1} - 10^{-2}$ , which is well below the lower critical value threshold favorable for shear-induced turbulence. The dissipation rate near the seabed in MS was close to  $\epsilon_b \approx 10^{-3} \text{ Wkg}^{-1}$ . Note that the tidally-induced near-bottom dissipation rate in the Puget Sound, WA, USA, reported by Thomson



March 5, St 3, 2<sup>nd</sup> cast      March 6, St 3, 1<sup>st</sup> cast

Fig. 9 The VMP sinking velocity profiles for two casts taken in the Magellan Strait on March 5 and 6, 2019 (see stations in Fig. 1)

et al. (2012) was as high as that measured in the Strait of Magellan, namely  $\epsilon_b \sim 10^{-4} - 10^{-3} \text{ W kg}^{-1}$ . During microstructure measurements, the tidally generated turbulent BBL height was  $\sim 4 - 7 \text{ m}$ , with an exponential decay of TKE dissipation rate and vertical shear vertically away from the bottom. In the exponentially varying regime, the eddy viscosity was found to be  $K_M = (0.83 - 3.4) \times 10^{-3} \text{ m}^2 \text{ s}^{-1}$ , independent of the vertical coordinate  $\xi$  but arguably dependent on tidal phase and location. Note that the eddy viscosity as high as  $10^{-2} - 10^{-1} \text{ m}^2\text{s}^{-1}$  has been reported by Ross et al. (2019) for the spring tide in a plain estuary on the French Atlantic Coast. The results of the pilot field campaign described in this paper provided first yet limited information on the turbulence structure in the north-eastern Magellan Strait, calling for further comprehensive investigations.

### Appendix

The VMP sinking velocity profiles

Examples of the VMP sinking velocity profiles  $W(P)$  shown in Fig. 9 indicate fairly undisturbed almost constant  $W(P) \sim 0.7 \text{ m/s}$  during a major portion of the casts and a sharp drop of  $W(P)$  to zero at the end of the casts ( $P$  is pressure).

**Acknowledgements** We are greatly thankful to the crew of the vessel Marypaz II for immense help during the VMP measurements. The research cruise was funded by the Marine Energy Research & Innovation Center of Chile (MERIC), CORFO project 14CEI2-28228. Chilean scientists were supported by MERIC and Research Internationalization Grant of the Pontificia Universidad Católica de Chile (grant no. PUC1566). The University of Notre Dame participants were partially supported through the 2018-2019 Luksic Family Collaboration Grant Award (<https://international.nd.edu/faculty-research/grants-and-funding/luksic-family-collaboration-grant/luksic-family-collaboration-grant-awardees/>). During the preparation of this paper, Notre Dame group was supported by ONR Grants N00014-23-1-2053 (dealing with Arabian sea air-sea interactions) as well as N00014-18-1-2472 and N00014-18-1-2472 (shelf/BBL turbulence with applications to marine fog genesis).

**Data availability** The data used in this paper is available upon request from the corresponding author. Data management repository available at [https://drive.google.com/drive/folders/1mVA--r4dQ9qVBgSmxNQILcQJ\\_5ypC\\_93?usp=sharing](https://drive.google.com/drive/folders/1mVA--r4dQ9qVBgSmxNQILcQJ_5ypC_93?usp=sharing).

## Declarations

**Competing interest** The authors declare no conflicts of known competing financial interest relevant to this study.

**Open Access** This article is licensed under a Creative Commons Attribution 4.0 International License, which permits use, sharing, adaptation, distribution and reproduction in any medium or format, as long as you give appropriate credit to the original author(s) and the source, provide a link to the Creative Commons licence, and indicate if changes were made. The images or other third party material in this article are included in the article's Creative Commons licence, unless indicated otherwise in a credit line to the material. If material is not included in the article's Creative Commons licence and your intended use is not permitted by statutory regulation or exceeds the permitted use, you will need to obtain permission directly from the copyright holder. To view a copy of this licence, visit <http://creativecommons.org/licenses/by/4.0/>.

## References

- Acevedo J, Plana J, Aguayo-Lobo A, Pastene LA (2011) Surface feeding behavior of humpback whales in the Magellan Strait. *Revista De Biología Marina y Oceanografía* 46(3):483–490. <https://doi.org/10.4067/S0718-19572011000300018>
- Antezana T (1999) Hydrographic features of Magellan and Fuegian inland passages and adjacent Subantarctic waters. *Sci Mar* 63(S1):23–74
- Antezana T, Hamamé M (1999) Short-term changes in the plankton of a highly homogeneous basin of the Straits of Magellan (Paso Ancho) during spring 1994. *Sci Mar* 63(S1):59–67
- Brun AA, Ramirez N, Pizarro O, Piola AR (2020) The role of the Magellan Strait on the southwest South Atlantic shelf. *Estuar., Coast. Shelf Sci* 237(106661):1–11. <https://doi.org/10.1016/j.ecss.2020.106661>
- Garreaud R, Lopez P, Minvielle M, Rojas M (2013) Large-scale control on the Patagonian climate. *J Climate* 26(1):215–230
- Goodman L, Levine ER, Lueck RG (2006) On measuring the terms of the turbulent kinetic energy budget from an AUV. *J. Atm. Ocean. Tech.* 23:977–990. <https://doi.org/10.1175/JTECH1889.1>
- Guerra M, Thomson J (2017) Turbulence measurements from five-beam acoustic doppler current profilers. *J Atm Ocean Tech* 34:1267–1284. <https://doi.org/10.1175/JTECH-D-16-0148.1>
- Gurvich AS, Yaglom AM (1967) Breakdown of eddies and probability distributions for small-scale turbulence. *Phys Fluids* 10:S59–S65. <https://doi.org/10.1063/1.1762505>
- Horwitz R, Hay A (2017) Turbulence dissipation rates from horizontal velocity profiles at mid-depth in fast tidal flows. *Renew Energy* 114:283–296. <https://doi.org/10.1016/j.renene.2017.03.062>
- Jinadasa SUP, Lozovatsky I, Planella-Morató J, Nash JD, MacKinnon JA, Lucas AJ, Wijesekera HW, Fernando HJS (2016) Ocean turbulence and mixing around Sri Lanka and in adjacent waters of the northern Bay of Bengal. *Oceanogr* 29:170–179. <https://doi.org/10.5670/oceanog.2016.49>
- Krstic A, Fernando HJS (2001) The nature of rough-wall oscillatory boundary layers. *J Hydraulic Res* 39(6):655–666. <https://doi.org/10.1080/00221686.2001.9628294>
- Lozovatsky I, Liu Z, Fernando HJS, Armengol J, Roget E (2012) Shallow water tidal currents in close proximity to the seafloor and boundary-induced turbulence. *Ocean Dyn* 62:177–201. <https://doi.org/10.1007/s10236-011-0495-3>
- Lozovatsky I, Lee J-H, Fernando HJS, Kang SK, Jinadasa SUP (2015) Turbulence in the East China Sea: The summertime stratification. *J Geophys Res Oceans* 120:1856–1871. <https://doi.org/10.1002/2014JC010596>
- Lozovatsky I, Planella-Morato J, Shearman K, Wang Q, Fernando HJS (2017a) Eddy diffusivity and elements of mesoscale dynamics over North Carolina shelf and contiguous Gulf Stream waters. *Ocean Dyn* 67:783–798. <https://doi.org/10.1007/s10236-017-1059-y>
- Lozovatsky I, Fernando HJS, Planella-Morato J, Liu Z, Lee J-H, Jinadasa SUP (2017b) Probability distribution of turbulent kinetic energy dissipation rate in ocean: Observations and approximations. *J Geophys Res Oceans* 122:8293–8308. <https://doi.org/10.1002/2017JC013076>
- Lozovatsky I, Pirro A, Jarosz E, Wijesekera HW, Jinadasa SUP, Fernando HJS (2019) Turbulence at the periphery of Sri Lanka dome. *Deep Sea Res II* 168(104614):1–8. <https://doi.org/10.1016/j.dsr2.2019.07.002>
- Lozovatsky I, Wainwright C, Creegan E, Fernando HJS (2021) Ocean turbulence and mixing near the shelf break southeast of Nova Scotia. *Bound Layer Met* 181:425–441. <https://doi.org/10.1007/s10546-020-00576-z>
- Lozovatsky ID, Liu Z, Hao W, Fernando HJS (2008) Tides and mixing in the northwestern East China Sea. Part II The near-bottom turbulence. *Cont Shelf Res* 28(2):338–350. <https://doi.org/10.1016/j.csr.2007.08.007>
- Lutz V, Frouin R, Negri R, Silva R, Pompeu M, Rudorff N, Cabral A, Dogliotti A, Martinez G (2016) Bio-optical characteristics along the Straits of Magallanes. *Cont Shelf Res* 119:56–67
- McMillan JM, Hay AE (2017) Spectral and structure function estimates of turbulence dissipation rates in a high-flow tidal channel using broadband ADCPs. *J Atm Oceanic Tech* 34:5–20. <https://doi.org/10.1175/JTECH-D-16-0131.1>
- McMillan JM, Hay AE, Lueck RG, Wolk F (2016) Rates of dissipation of turbulent kinetic energy in a high Reynolds number tidal channel. *J Phys Oceanog* 33:817–837. <https://doi.org/10.1175/JTECH-D-15-0167.1>
- Medeiros C, Kjerfve B (1988) Tidal characteristics of the Strait of Magellan. *Cont Shelf Res* 8(8):947–960
- Monin AS, Yaglom AM (1971) *Statistical Fluid Mechanics: Mechanics of Turbulence*, 1. MIT Press, Cambridge, MA, p 782
- Moum JN, Caldwell DR, Nash JD, Gunderson GD (2002) Observations of boundary mixing over the continental slope. *J Phys Oceanogr* 32:2113–2130
- Pedlosky J (1987) *Geophysical Fluid Dynamics*. 2nd ed. Springer-Verlag, 710 <https://doi.org/10.1007/978-1-4612-4650-3>
- Roget E, Lozovatsky I, Sanchez X, Figueroa M (2006) Microstructure measurements in natural waters: Methodology and applications. *Prog in Oceanogr* 70:123–148

- Ross L, Huguenard K, Sottolichio A (2019) Intratidal and fortnightly variability of vertical mixing in a macrotidal estuary: The Gironde. *J Geophys Res Oceans* 124:2641–2659. <https://doi.org/10.1029/2018JC014456>
- Sakamoto K, Akitomo K (2006) Instabilities of the tidally induced bottom boundary layer in the rotating frame and their mixing effect. *Dyn Atmos Oceans* 41:191–211
- Sakamoto K, Akitomo K (2008) The tidally induced bottom boundary layer in a rotating frame: similarity of turbulence. *J Fluid Mech* 615:1–25. <https://doi.org/10.1017/S0022112008003340>
- Sanford TS, Lien R-C (1999) Turbulent properties in a homogeneous tidal boundary layer. *J Geophys Res Oceans* 104(C1):1245–1257
- Simeoni U, Fontolan G, Colizza E (1997) Geomorphological characterization of the coastal and marine area between Primera and Segunda Angostura, Strait of Magellan (Chile). *J Coastal Res* 13(3):916–924
- St. Laurent LC, Simmons HL, Jayne SR (2002) Estimating tidally driven mixing in the deep ocean. *Geophys Res Lett* 29(23): 21-1-21-4. <https://doi.org/10.1029/2002GL015633>
- St. Laurent LC, Toole JM, Schmitt RW, (2001) Buoyancy forcing by turbulence above rough topography in the abyssal Brazil Basin. *J Phys Oceanogr* 31(12):3476–3495. [https://doi.org/10.1175/1520-0485\(2001\)031<3476:BFBTAR>2.0.CO;2](https://doi.org/10.1175/1520-0485(2001)031<3476:BFBTAR>2.0.CO;2)
- Stevens CL, Smith MJ (2016) Turbulent mixing in a stratified estuarine tidal channel: Hikapu Reach, Pelorus Sound, New Zealand, New Zealand *J Marine and Freshwater Res* 50(4):485–505. <https://doi.org/10.1080/00288330.2016.1171243>
- Thomson J, Polagye B, Durgesh V, Richmond MC (2012) Measurements of turbulence at two tidal energy sites in Puget Sound. *WA IEEE J Oceanic Eng* 37(3):363–374. <https://doi.org/10.1029/2010GL044156>
- Wolk F, Lueck R (2012) VMP turbulence profiler measurements in a tidal channel. Rockland Tech Note 024. Published on 2012-06-30. [https://rocklandscientific.com/wp-content/uploads/2021/12/TN\\_024\\_VMP\\_in\\_Tidal\\_Channels.pdf](https://rocklandscientific.com/wp-content/uploads/2021/12/TN_024_VMP_in_Tidal_Channels.pdf)
- Yoshikawa Y, Endoh T, Matsuno T, Wagawa T, Tsutsumi E, Yoshimura H, Morii Y (2010) Turbulent bottom Ekman boundary layer

measured over a continental shelf. *Geophys Res Lett* 37:L15605. <https://doi.org/10.1029/2010GL044156>

#### Postscript: In Memoriam

The lead author of this paper, Iossif D. Lozovatsky, a research professor of civil and environmental engineering and earth sciences at University of Notre Dame, passed away on 23 December 2023. He was 75. This is the final paper that Professor Lozovatsky has led and revised. An expert in physical oceanography, his research lab was the world's oceans, seas and lakes. Born in Kiev, Ukraine, Lozovatsky received a master's degree in oceanography from Lomonosov Moscow State University and a doctorate in physics and mathematics from the Shirshov Institute of Oceanology, where he later became a full professor and lead research scientist. He joined Arizona State University's Center for Environmental Fluid Dynamics in 1994, and in 2010 moved to University of Notre Dame's Environmental Fluid Dynamics Laboratory as a research professor. He worked with collaborators from around the world, making more than 20 oceanographic research cruises in the Atlantic, Pacific, Indian and Antarctic oceans as well as the Baltic, Black, Mediterranean and China Seas. His collaborations included University of Girona in Spain, the University of Western Australia in Perth, the Ocean University of China in Quindao, the State Key Laboratory of Marine Environmental Science and Xiamen University in Xiamen and the National Aquatic Resources Research and Development Agency (NARA) in Colombo, Sri Lanka. Professor Lozovatsky has published more than 100 papers in international journals, covering small-scale physical oceanography and aspects of atmospheric science and fluid dynamics. He also was known as a gifted teacher, deepening graduate students' understanding of their field by providing meticulous training and insightful questioning. He will be sorely missed!